Chapter 4
Implementation of Local Stochastic Volatility Model in FX Derivatives

J. Zheng and X. Yuan

Abstract In this paper, we present our implementations of the Local Stochastic Volatility (LSV) Model in pricing exotic options in FX Market. Firstly, we briefly discuss the limitations of the Black-Scholes model, the Local Volatility (LV) Model and the Stochastic Volatility (SV) Model. To overcome the drawbacks of the above three models, a more generalized LSV model has been proposed to describe the dynamics of implied volatilities. Secondly, we present the details of LSV Model calibration in terms of the Forward Kolgomorov equation. Thirdly, we introduce the numerical methods of option pricing using the LSV model, including both the Backward Partial Differential Equation (PDE) method and Forward Monte Carlo method. Finally, based on our implementations, we compare the calibration and pricing results of the LSV model with the LV model and the SV model, lower calibration errors and relatively accurate pricing results are achieved, which demonstrates the effectiveness of the methods presented in the paper.

4.1 Introduction

Traditional Black-Scholes model (Black and Scholes 1973) is broadly used in European vanilla option pricing for both FX and equity markets. In the Black-Scholes model for FX market, the FX spot rate S_t is assumed to follow the Stochastic Differential Equation (SDE) as below

$$dS_t = \left(r_d - r_f\right) S_t dt + \sigma S_t dW_t \tag{4.1}$$

J. Zheng (✉) · X. Yuan
Global Market Department, Industrial and Commercial Bank of China,
Peking, People's Republic of China
e-mail: zhjune@gmail.com, jun.zheng@icbc.com.cn

X. Yuan
e-mail: yuanxun@ustc.edu

W.K. Härdle et al. (eds.), *Applied Quantitative Finance*, Statistics and Computing,
DOI 10.1007/978-3-662-54486-0_4

where r_d and r_f denote the domestic interest rate and the foreign interest rate respectively, and volatility σ is assumed to be constant.

However, in real market (e.g. the FX market), the volatility is not constant across different strikes and maturity dates, which is quite important for pricing barrier options. To tackle the problem of volatility smile and to describe the dynamics of implied volatilities, several models have been developed to generalize Black-Scholes model.

The Local Volatility (LV) model was firstly proposed by Dupire (1994). In the LV model, the diffusion coefficient is a deterministic function of time and the FX spot rate, $\sigma_{LV}(S_t, t)$, the corresponding SDE is as below

$$dS_t = \left(r_d - r_f\right) S_t dt + \sigma_{LV}(S_t, t) S_t dW_t \tag{4.2}$$

Theoretically, the LV model is able to provide a perfect fit to the quoted market implied volatilities. However, it still has several drawbacks. Firstly, it has been pointed out that the delta of an option computed from the LV model is far away from precise, because of an improper implied volatility dynamics (Hagan et al. 2002). Secondly, the forward implied volatility smile generated by the LV model is almost flat (Fengler 2005), but the smile persists over time in the reality. Thirdly, the LV model generates the volatility smile using a deterministic function $\sigma_{LV}(S_t, t)$, which depends on the spot level S_t. Therefore, the LV model is sticky-strike, which seldom happened in the FX market (Clark 2011).

Based on an empirical observation of FX market, it is more reasonable to model the instaneous volatility via a stochastic process, which leads to the Stochastic Volatility (SV) model. In a SV model, the diffusion coefficient is a function of a stochastic process v_t, $a(v_t)$, the corresponding SDE is as following

$$dS_t = \left(r_d - r_f\right) S_t dt + a(v_t) S_t dW_t \tag{4.3a}$$

$$dv_t = b(v_t) dt + c(v_t) dZ_t \tag{4.3b}$$

$$dW_t dZ_t = \rho dt$$

where ρ represents the correlation between the Brownian motions W_t and Z_t. In most cases, the stochastic variance v_t is assumed to be mean-reverting, continuous, and positive. For example, in the well-known Heston model (Heston 1993), the Cox-Ingersoll-Ross (CIR) process is used to model the variance process v_t:

$$dS_t = \left(r_d - r_f\right) S_t dt + \sqrt{v_t} S_t dW_t \tag{4.4a}$$

$$dv_t = \kappa (m - v_t) dt + \alpha \sqrt{v_t} dZ_t \tag{4.4b}$$

$$dW_t dZ_t = \rho dt$$

where κ is the mean-reverting speed, m is the mean-reverting level, and α corresponds to the volatility of variance. Compared with the LV model, the SV model is able to imply a more realistic forward implied volatility smile. However, it still has several drawbacks. Firstly, the SV model is not able to fit the implied volatility

surface perfectly as the LV does. Secondly, the SV model generates the same smile irrespective of initial level of the spot, and is therefore "sticky-delta", which is not the reality in FX market either (Clark 2011).

To overcome the drawbacks of the LV model and the SV model, a more generalized model, named Local Stochastic Volatility (LSV) model was introduced. In the LSV model, the diffusion coefficient is the multiplication of a deterministic local volatility component $\sigma_{LSV}(S_t, t)$ and a stochastic volatility component v_t. For example, the SDE for a Heston-type LSV model is as below.

$$dS_t = \left(r_d - r_f\right) S_t dt + \sigma_{LSV}(S_t, t)\sqrt{v_t} S_t dW_t \tag{4.5a}$$

$$dv_t = \kappa(m - v_t)dt + \alpha\sqrt{v_t} dZ_t \tag{4.5b}$$

$$dW_t dZ_t = \rho dt$$

In the LSV model, part of the volatility smile is generated by the deterministic local volatility term $\sigma_{LSV}(S_t, t)$, while the rest part of the smile is generated by the stochastic volatility term v_t. Therefore, the LSV model is the model between"sticky-delta" and "sticky-strike", which is actually useful in the FX market. Moreover, it fits the implied volatility surface quite well as the LV model does, and meanwhile implies a more realistic forward implied volatility smile assumed by the SV model.

The rest of this paper is organized as following. In Sect. 4.2, we detail the LSV model calibration process through solving a Fokker–Planck Equation (FPE) iteratively. In Sect. 4.3, two different numerical methods for pricing exotic options using the LSV model are introduced, Backward PDE, and Forward Monte Carlo. Numerical results for model calibration and barrier option pricing are presented in Sect. 4.4, followed by the conclusion remarks and future works in Sect. 4.5.

4.2 Model Calibration

As mentioned in Sect. 4.1, by choosing different stochastic processes for v_t, we can get different types of the LSV model. For simplicity, we limit our discussions to Heston-type LSV model. The calibration of other types of LSV model can be performed similarly.

Generally speaking, the calibration of the LSV model consists of two main steps. In step 1, the parameters of the SV part are calibrated to fit a certain proportion of volatility smile. The proportion is controlled by a mixing fraction parameter, which is between 0 and 1. In step 2, the parameters of LV part are added to calibrate the LSV model to the whole volatility smile.

Step 1: Calibrate the parameters for the SV part, this step is performed infrequently. Specify a mixing weight η, which controls the proportion of volatility smile generated by the SV part and the proportion generated by the LV part. The mixing weight is used to mark down the implied volatility smile and skew, which can be done in two ways. One way is to multiply the market quotes of Butterfly and Risk Reversal by the factor

η. The Butterfly quotes correspond to the volatility smile, while the Risk Reversal quotes correspond to the volatility skew. Since the multiplication will reduce the volatility smile and skew, we calibrate a purely SV model to the market quotes with a reduced smile and skew. The other way is to calibrate a purely SV model to the true market quotes firstly, and then multiply the volatility of variance α and correlation ρ by the factor η, because the volatility of variance parameter corresponds to the volatility smile, and the correlation parameter corresponds to the volatility skew.

Step 2: Calibrate the leverage function $\sigma_{LSV}(S_t, t)$ so that the LSV model can fit the market quotes of vanilla options. This step is usually performed more frequently than step 1. We will detail the implementations of this step in the later part of this Section.

In our experiments, we set the mixing fraction empirically as described in Clark (2011). However, please note that the mixing fraction can also be calibrated using the quoted prices of liquid barrier options, as described in Tian (1993).

The calculation of the leverage function $\sigma_{LSV}(S_t, t)$ is based on the following important result: there exists only one LSV surface $\sigma_{LSV}(S_t, t)$ so that the LSV model can mimic the LV model, and $\sigma_{LSV}(S_t, t)$ must follow

$$\sigma_{LV}(s,t)^2 = E\left[\sigma_{LSV}(s,t)^2 v_t \mid S_t = s\right] = \sigma_{LSV}(s,t)^2 E\left[v_t \mid S_t = s\right] \tag{4.6}$$

For the proof the above important result, please refer to Ren et al. (2007), Tachet (2011). Based on the result, we can compute $\sigma_{LSV}(S_t, t)$ as the ratio between local volatility and conditional expectation of stochastic volatility:

$$\sigma_{LSV}(s,t) = \frac{\sigma_{LV}(s,t)}{\sqrt{E\left[v_t \mid S_t = s\right]}} = \sigma_{LV}(s,t)\sqrt{\frac{\int_v p(s,v,t)\,dv}{\int_v v \cdot p(s,v,t)\,dv}} \tag{4.7}$$

where $\sigma_{LV}(S_t, t)$ can be acquired from the LV model. Therefore, the key of calculating $\sigma_{LSV}(S_t, t)$ is to compute the joint probability distribution $p(s, v, t)$. Ren, Madan, and Qian (2007) firstly proposed to calculate $p(s, v, t)$ by solving the Fokker–Planck Equation (FPE) of the LSV model through a Finite Difference Method. After their pioneering work, Tachet (2011), Tian (1993), and Clark (2011) also solved the FPE with the Finite Difference Method, while Engelmann (2012) used the finite volume method, and Cozzi (2012) used the finite element method.

Let $X_t = \ln(S_t)$, the FPE for Heston-type LSV is as following

$$\begin{aligned}\frac{\partial p}{\partial t} = {} & \frac{1}{2}\frac{\partial^2\left[v\sigma_{LSV}^2(X,t)\,p\right]}{\partial X^2} + \rho\alpha\frac{\partial^2\left[v\sigma_{LSV}(X,t)\,p\right]}{\partial X\partial v} + \frac{1}{2}\alpha^2\frac{\partial^2[vp]}{\partial v^2} \\ & + \frac{\partial}{\partial X}\left[\left(\frac{1}{2}v\sigma_{LSV}^2(X,t) - \left(r_d - r_f\right)\right)p\right] + \kappa\frac{\partial\left[(v-m)\,p\right]}{\partial v}\end{aligned} \tag{4.8}$$

where, for simplicity, $\sigma_{LSV}(S_t, t) = \sigma_{LSV}(X_t, t)$ refers to the leverage function of LSV model either in logspot or spot coordinates.

To solve the FPE (4.8), an Alternating-Direction-Implicit (ADI) method is used. Tataru and Fisher (2010) suggest to use a modified Douglas scheme, which was used

by Hout and Foulson (2010) to solve the Backward pricing PDE for Heston model. The modified Douglas scheme is as below.

$$\begin{aligned} Y_0 &= p_{n-1} + \Delta t \left[F_0 \left(p_{n-1}, t_{n-1} \right) + F_1 \left(p_{n-1}, t_{n-1} \right) + F_2 \left(p_{n-1}, t_{n-1} \right) \right] \\ Y_1 - \theta \Delta t F_1 \left(Y_1, t_n \right) &= Y_0 - \theta \Delta t F_1 \left(p_{n-1}, t_{n-1} \right) \\ Y_2 - \theta \Delta t F_2 \left(Y_2, t_n \right) &= Y_1 - \theta \Delta t F_2 \left(p_{n-1}, t_{n-1} \right) \\ p_n &= Y_2 \end{aligned} \tag{4.9}$$

where p_n denotes the transition probability $p\left(s, v, t_n\right)$ at time t_n. The parameter θ affects the stability and accuracy of the ADI method, which lies in the range $[0, 1]$. F_0, F_1, and F_2 refer to derivative terms in mixed derivative, v-direction, and X-direction respectively.

$$\begin{aligned} F_0 \left(p, t \right) &= \rho \alpha \frac{\partial^2 \left[v \sigma_{LSV} \left(X, t \right) p \right]}{\partial X \partial v} \\ F_1 \left(p, t \right) &= \frac{1}{2} \alpha^2 \frac{\partial^2 \left[v p \right]}{\partial v^2} + \kappa \frac{\partial \left[(v - m) p \right]}{\partial v} \\ F_2 \left(p, t \right) &= \frac{1}{2} \frac{\partial^2 \left[v \sigma_{LSV}^2 \left(X, t \right) p \right]}{\partial X^2} + \frac{\partial}{\partial X} \left[\left(\frac{1}{2} v \sigma_{LSV}^2 \left(X, t \right) - \left(r_d - r_f \right) \right) p \right] \end{aligned} \tag{4.10}$$

The initial value for the FPE is $p_0 = p\left(X, v, 0\right) = \delta\left(X - X_0\right) \delta\left(v - v_0\right)$, where the $\delta()$ is the Dirac Delta function. According to Eq. (4.7), the leverage function at time zero is $\sigma_{LSV}\left(X_0, 0\right) = \frac{\sigma_{LV}\left(X_0, 0\right)}{\sqrt{v_0}}$. At time t_n, we have p_n and $\sigma_{LSV}\left(X, t_n\right)$, then we can solve FPE (4.8) forward one step to get p_{n+1}, and then use Eq. (4.7) to get the leverage function $\sigma_{LSV}\left(X, t_{n+1}\right)$ at time t_{n+1}. This process is repeated through time, and we can solve p_n and $\sigma_{LSV}\left(X, t_n\right)$ for all time points:

The solved $\sigma_{LSV}\left(X, t\right)$ can be used to price derivative products, either by a backward PDE or a forward Monte Carlo approach. We will detail the two pricing methods for the LSV model in the next section (Fig. 4.1).

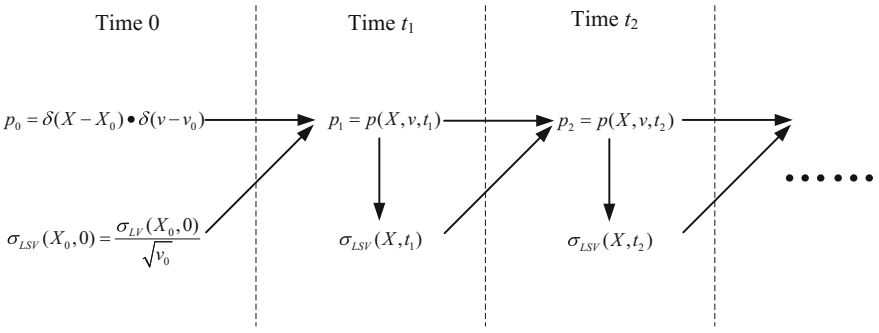

Fig. 4.1 Solve the FPE Iteratively to get the Leverage Function $\sigma_{LSV}\left(X, t\right)$

4.3 Pricing (Backward PDE and Forward Monte Carlo)

Let $V(X, v, t)$ denotes the option value as a function of time to expiry t, log-Spot level X, and the instaneous variance v. The backward pricing PDE for Heston-type LSV model are as following.

$$\begin{aligned}\frac{\partial V}{\partial t} &= \frac{1}{2}v\sigma_{LSV}^2(X,t)\frac{\partial^2 V}{\partial X^2} + \frac{1}{2}\alpha^2 v\frac{\partial^2 V}{\partial v^2} + \rho\alpha v\sigma_{LSV}(X,t)\frac{\partial^2 V}{\partial X\partial v} \\ &+ \left(r_d - r_f - \frac{1}{2}v\sigma_{LSV}^2(X,t)\right)\frac{\partial V}{\partial X} + \kappa(m-v)\frac{\partial V}{\partial v} - r_d V \end{aligned} \tag{4.11}$$

Note that $t = 0$ corresponds to the option expiry, and $t = T$ corresponds to today. This is different from the FPE in Sect. 4.2, where we use $t = 0$ for today, and $t = T$ for option expiry.

We can also solve the backward pricing PDE using the modified Douglas scheme as shown in Eq. (4.9). Instead, the mixed derivative operator F_0, v-direction derivative operator F_1, and X-direction derivative operator F_2 for the pricing PDE are as follow.

$$\begin{aligned} F_0(V,t) &= \rho\alpha v\sigma_{LSV}(X,t)\frac{\partial^2 V}{\partial X\partial v} \\ F_1(V,t) &= \frac{1}{2}\alpha^2 v\frac{\partial^2 V}{\partial v^2} + \kappa(m-v)\frac{\partial V}{\partial v} - \frac{1}{2}r_d V \\ F_2(V,t) &= \frac{1}{2}v\sigma_{LSV}^2(X,t)\frac{\partial^2 V}{\partial X^2} + \left(r_d - r_f - \frac{1}{2}v\sigma_{LSV}^2(X,t)\right)\frac{\partial V}{\partial X} - \frac{1}{2}r_d V \end{aligned} \tag{4.12}$$

In the backward pricing PDE, we start from the terminal condition, i.e., the payoff at expiry ($t = 0$). Based on the pricing PDE and some boundary conditions, we can propagate $V(X, v, t)$ backward to today ($t = T$), where we get the option value $V(X_T, v_T, T)$ by interpolation. The terminal condition and other boundary conditions are all determined by the option characteristics.

Besides the backward pricing PDE method, Monte Carlo method (Glasserman 2003) can also be utilized to price the options based on the LSV model. One key problem of Monte Carlo method for the LSV model is the discretization scheme of the SDE (4.5) for LSV model. A tradeoff between the computation complexity and accuracy should be found in the discretization scheme. Let $X_t = \ln(S_t)$, Eq. (4.5) can be rewritten as follow.

$$dX_t = \left[r_d - r_f - \frac{1}{2}V_t\sigma_{LSV}^2(X_t,t)\right]dt + \sigma_{LSV}(S_t,t)\sqrt{V_t}\left(\rho dW_v(t) + \sqrt{1-\rho^2}dW_x(t)\right) \tag{4.13a}$$

$$dV_t = \kappa(m - V_t)\,dt + \alpha\sqrt{V_t}dW_v(t) \tag{4.13b}$$

where $dW_x(t)$ and $dW_v(t)$ denote independent Brownian motions. When Feller condition $2\kappa m \geq \alpha^2$ is not satisfied, the variance process can become negative

with non-zero probability in the Euler discretization. Therefore, we adopt the QE (Quadratic Exponential) (Andersen 2008) scheme for the discretization of the variance process. For the discretization of the log-spot process, we adopt the local-freezing of $\sigma_{LSV(X,t)}$, introduced by Van etc. (2014). More specifically, the discretization scheme for log-spot process is as follow.

$$x_{i+1} = x_i + r\Delta - \frac{1}{2}\sigma^2_{LSV}\left(x_i, t_i\right) v_i \Delta + \frac{\rho}{\alpha}\sigma^2_{LSV}\left(x_i, t_i\right)\left(v_{i+1} - \kappa m \Delta + v_i c_1\right) + Z_x \cdot \sqrt{1-\rho^2} \cdot \sqrt{\sigma^2_{LSV}\left(x_i, t_i\right) v_i \Delta} \tag{4.14}$$

where $Z_x \sim N(0, 1)$, $c_1 = \kappa\Delta - 1$.

4.4 Empirical Results

For the implementations of LSV model, one strives to solve the FPE accurately with low calibration errors w.r.t the market prices of vanilla options. In our empirical results, the low calibration errors for LSV model are achieved, which demonstrate the effectiveness of the methods presented in this paper. Moreover, we also compare the pricing results of reverse knock-out barrier options using the LV, the SV, and the LSV respectively. Among the three models, the price derived from the LSV model is the closest one to the market prices.

As a representative example, we calibrate the LV model (Dupire model), the SV model (Heston model), and the LSV model (as described above, its SV part is Heston-type) from market data in June 22, 2016 (data source: Bloomberg Terminal). Both the calibrated model parameters and calibration errors for the three models are discussed as following.

The implied volatility market data is shown in Table 4.1, while in Table 4.2 we present the calibrated implied volatilities of LV model with corresponding errors in the bracket. One can see that the calibration errors are very small, suggesting that the LV model is able to provide a perfect fit to the quoted market implied volatilities, as stated in Sect. 4.1. Theoretically the errors can be zero, however in practice there are usually some small errors remained when numerical methods are used. The model parameter, i.e. leverage surface $\sigma_{LV}(S_t, t)$ in the LV model is shown in Fig. 4.2.

The calibrated implied volatilities of the Heston model, with corresponding errors in the bracket, is shown in Table 4.3. Comparing Tables 4.2 and 4.3, we can find that the calibration errors for the Heston model are larger than LV model, which demonstrates that the Heston model is not able to fit the implied volatility surface perfectly as the LV does, as stated in Sect. 4.1. The corresponding model parameters for Heston model is shown in Table 4.4.

In Table 4.5, we present the calibrated implied volatilities of the LSV model with corresponding errors in the bracket. Comparing Tables 4.2, 4.3 and 4.5, one can find that the LSV model and the LV model can achieve much lower calibration errors than

Table 4.1 EUR/USD market implied volatility (in%)

Maturity	10-Delta put	25-Delta put	ATM	25-Delta call	10-Delta call
1W	22.554	19.756	17.333	15.944	15.531
2W	17.814	15.585	13.505	12.42	12.111
3W	16.466	14.176	12.217	11.304	11.334
1M	15.135	13.334	11.555	10.676	10.375
6W	14.463	12.744	11.049	10.231	10.023
2M	13.304	11.725	10.175	9.465	9.416
3M	12.894	11.298	9.855	9.302	9.416
4M	12.897	11.272	9.841	9.315	9.475
5M	12.901	11.243	9.825	9.33	9.542
6M	12.905	11.215	9.81	9.345	9.61
9M	12.79	11.088	9.733	9.32	9.662
1Y	12.666	10.951	9.65	9.294	9.719
18M	12.58	10.971	9.793	9.519	9.94
2Y	12.478	10.99	9.885	9.67	10.083

Table 4.2 Calibrated implied volatility of the LV model for EUR/USD (in%)

Maturity	10-Delta put	25-Delta put	ATM	25-Delta call	10-Delta call
1W	22.534[−0.020]	19.799[0.043]	17.255[−0.078]	15.919[−0.025]	15.525[−0.006]
2W	18.259[0.445]	16.007[0.422]	13.813[0.308]	12.726[0.306]	12.413[0.302]
3W	16.765[0.299]	14.481[0.305]	12.427[0.210]	11.513[0.209]	11.513[0.179]
1M	15.406[0.271]	13.579[0.245]	11.666[0.111]	10.799[0.123]	10.533[0.158]
6W	14.303[−0.160]	12.630[−0.114]	10.889[−0.160]	10.081[−0.150]	9.884[−0.139]
2M	13.550[0.246]	11.963[0.238]	10.355[0.180]	9.636[0.171]	9.575[0.159]
3M	12.960[0.066]	11.371[0.073]	9.866[0.011]	9.320[0.018]	9.434[0.018]
4M	12.867[−0.030]	11.288[0.016]	9.818[−0.023]	9.326[0.011]	9.475[0.000]
5M	12.915[0.014]	11.286[0.043]	9.858[0.033]	9.379[0.049]	9.585[0.043]
6M	12.944[0.039]	11.256[0.041]	9.799[−0.011]	9.347[0.002]	9.623[0.013]
9M	12.572[−0.218]	10.926[−0.162]	9.593[−0.140]	9.216[−0.104]	9.545[−0.117]
1Y	12.687[0.021]	10.975[0.024]	9.641[−0.009]	9.296[0.002]	9.723[0.004]
18M	12.736[0.156]	11.120[0.149]	9.883[0.090]	9.615[0.096]	10.042[0.102]
2Y	12.491[0.013]	11.003[0.013]	9.870[−0.015]	9.665[−0.005]	10.085[0.002]

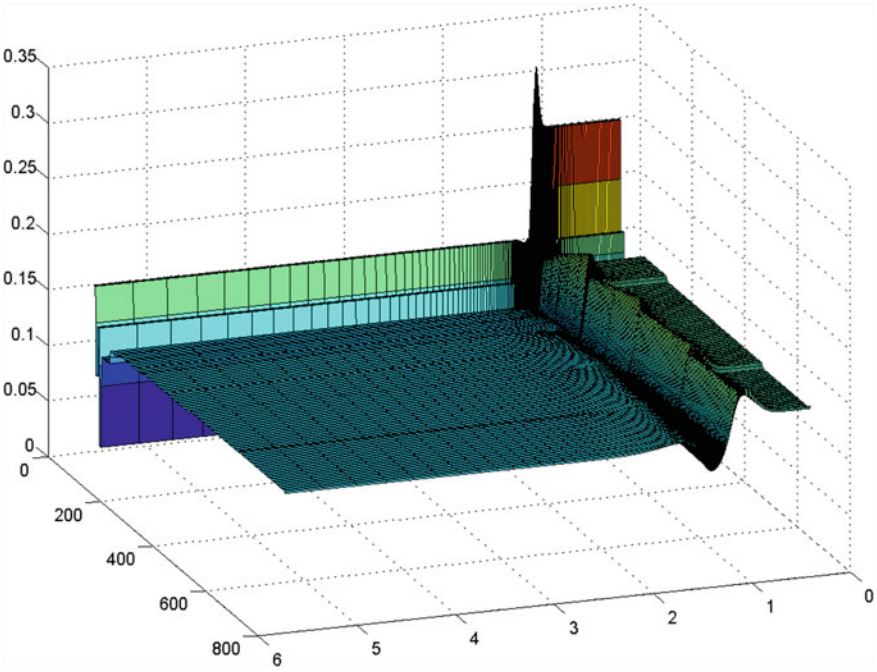

Fig. 4.2 Leverage surface in LV Model for EUR/USD

Table 4.3 Calibrated implied volatility of the heston model for EUR/USD (in%)

Maturity	10-Delta put	25-Delta put	ATM	25-Delta call	10-Delta call
1W	14.797[−7.757]	13.681[−6.075]	12.772[−4.561]	12.223[−3.721]	12.003[−3.528]
2W	14.819[−2.995]	13.558[−2.027]	12.515[−0.990]	11.926[−0.494]	11.752[−0.359]
3W	14.906[−1.560]	13.455[−0.721]	12.270[0.053]	11.648[0.344]	11.544[0.210]
1M	14.874[−0.261]	13.332[−0.002]	12.008[0.453]	11.369[0.693]	11.341[0.966]
6W	14.904[0.441]	13.146[0.402]	11.628[0.579]	10.989[0.758]	11.095[1.072]
2M	14.711[1.407]	12.797[1.072]	11.172[0.997]	10.566[1.101]	10.792[1.376]
3M	14.538[1.644]	12.384[1.086]	10.611[0.756]	10.063[0.761]	10.488[1.072]
4M	14.416[1.519]	12.107[0.835]	10.241[0.400]	9.742[0.427]	10.291[0.816]
5M	14.247[1.346]	11.828[0.585]	9.908[0.083]	9.455[0.125]	10.101[0.559]
6M	14.104[1.199]	11.629[0.414]	9.692[−0.118]	9.269[−0.076]	9.970[0.360]
9M	13.666[0.876]	11.171[0.083]	9.266[−0.467]	8.885[−0.435]	9.641[−0.021]
1Y	13.316[0.650]	10.878[−0.073]	9.036[−0.614]	8.664[−0.630]	9.418[−0.301]
18M	12.853[0.273]	10.565[−0.406]	8.831[−0.962]	8.460[−1.059]	9.167[−0.773]
2Y	12.535[0.057]	10.399[−0.591]	8.763[−1.122]	8.378[−1.292]	9.017[−1.066]

Table 4.4 Heston model parameters for EUR/USD

Initial variance	0.017
Mean-reverting speed κ	2.486
Mean-reverting level m	0.00953
Vol of variance α	0.57
Correlation ρ	−0.4

Table 4.5 Calibrated implied volatility of LSV model for EUR/USD (in%)

Maturity	10-Delta put	25-Delta put	ATM	25-Delta call	10-Delta call
1W	22.097[−0.457]	19.482[−0.274]	16.998[−0.335]	15.711[−0.233]	15.338[−0.193]
2W	17.868[0.054]	15.653[0.068]	13.520[0.015]	12.481[0.061]	12.203[0.092]
3W	16.502[0.036]	14.248[0.072]	12.240[0.023]	11.357[0.053]	11.384[0.050]
1M	15.233[0.098]	13.434[0.100]	11.555[0.000]	10.719[0.043]	10.463[0.088]
6W	14.215[−0.248]	12.554[−0.190]	10.833[−0.216]	10.056[−0.175]	9.888[−0.135]
2M	13.419[0.115]	11.853[0.128]	10.270[0.095]	9.575[0.110]	9.531[0.115]
3M	12.997[0.103]	11.425[0.127]	9.923[0.068]	9.387[0.085]	9.505[0.089]
4M	12.915[0.018]	11.352[0.080]	9.882[0.041]	9.391[0.076]	9.543[0.068]
5M	12.954[0.053]	11.355[0.112]	9.930[0.105]	9.449[0.119]	9.645[0.103]
6M	12.946[0.041]	11.279[0.064]	9.815[0.005]	9.359[0.014]	9.628[0.018]
9M	12.779[−0.011]	11.150[0.062]	9.788[0.055]	9.374[0.054]	9.679[0.017]
1Y	12.645[−0.021]	10.936[−0.015]	9.566[−0.084]	9.191[−0.103]	9.617[−0.102]
18M	12.500[−0.080]	10.879[−0.092]	9.606[−0.187]	9.313[−0.206]	9.741[−0.199]
2Y	12.414[−0.064]	10.916[−0.074]	9.735[−0.150]	9.492[−0.178]	9.899[−0.184]

the Heston model does. Theoretically, the LV model and the LSV model are more likely to achieve zero calibration errors, whereas the Heston model can't. In practice, there are still some small errors remained for the LV model and the LSV model due to numerical methods. Usually these numerical errors of the LSV model are larger than the LV model, because the LSV model involves more complex numerical methods than the LV model. In Table 4.5, the calibration errors for LSV model are very low, which demonstrate the effectiveness of the numerical methods presented in Sects. 4.2 and 4.3.

The model parameters for the SV part of the LSV model are acquired from the calibrated Heston model, except that the volatility of variance is multiplied by the mixing fraction parameter, which is set to 0.4 here. The model parameter, i.e. leverage surface $\sigma_{LSV}(S_t, t)$ in the LSV model is shown in Fig. 4.3.

As stated above, the key problem of the LSV model implementations is to solve the FPE accurately to get low calibration errors. The FPE (4.8) is about the transition probability p. To show the numerical stability, we export the time evolution of the transition probability p in Eq. (4.8) to Fig. 4.4. From Fig. 4.4, we can see that the evolution of transition probability is stable. It is noted that for numerical stability,

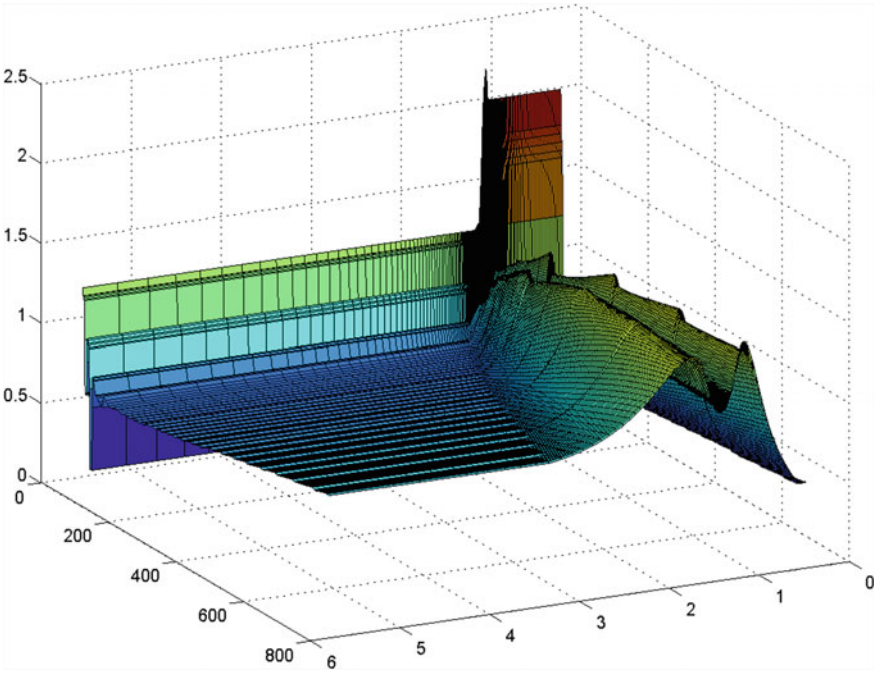

Fig. 4.3 Leverage surface in LSV Model for EUR/USD

we make the following transformation to spot s and variance v when calculating Eq. (4.8) numerically: $Y_t = \ln(S_t/S_0)$, $Z_t = \ln(V_t/V_0)$.

We also compare the pricing results of reverse knock-out barrier options, which are up-and-out single-barrier call options, and traded quite frequently in the market. The pricing method is the backward PDE introduced in Sect. 4.3. The prices of the three different models, as well as the market prices, are summarized in Table 4.6. The market prices are collected from Bloomberg. We can see that the LSV model provides the prices which are closest to the market prices.

4.5 Conclusion and Future Works

In this paper, we detail our implementations of a Heston-type LSV model. The model calibration is based on solving a Fokker–Planck Equation iteratively. For derivatives pricing, both the backward PDE method and Forward Monte Carlo method are introduced. In numerical results, the low calibration errors and relatively accurate pricing results demonstrate the effectiveness of the methods presented in this paper. For future works, the most important task is to improve the calibration stability. In our implementations, we face the similar problem described in Ait (2013): the calibration

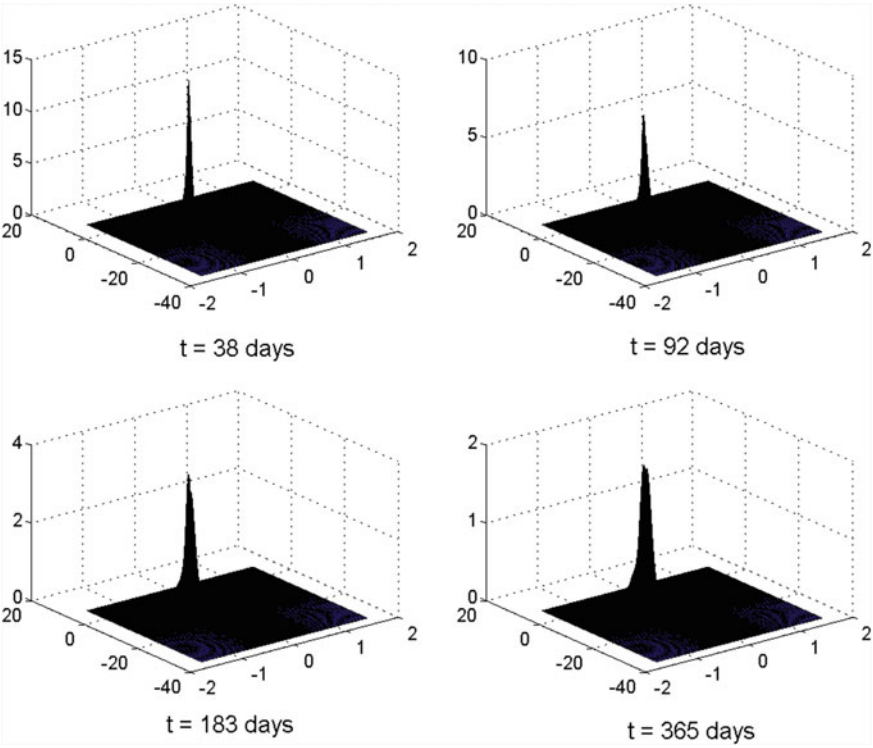

Fig. 4.4 Time evolution of the transition probability

Table 4.6 Pricing results of reverse knock-out barrier options

Tenor	Strike	Barrier	Heston	LV	LSV	Market price
1M	1.1269	1.15	1430	962	1054	1035
1M	1.1269	1.17	6001	5920	6072	5997
3M	1.1293	1.16	2262	922	1173	1087
3M	1.1293	1.2	10855	9287	9812	9901
6M	1.1331	1.19	6925	3328	4323	3883
6M	1.1331	1.24	16907	14170	15322	15102
1Y	1.1417	1.22	9787	4477	6103	5212
1Y	1.1417	1.3	25057	20601	22530	21936

becomes instable for large volatility-of-variance and longer maturity. Two ways are supposed to improve the calibration stability: one is to add a zero-flux boundary condition when solving the FPE (Lucic 2013; Gottker and Spanderen 2014); the other is to perform forward induction of backward PDE (Andreasen and Huge 2010).

References

Ait, Z. (2013). Alternate direction implicit method for a stochastic local volatility model: High performance computing platforms comparison.

Andersen, L. (2008). Simple and efficient simulation of the heston stochastic volatility model. *Journal of Computational Finance*, *11*, 1–42.

Andreasen, J., & Huge, B. N. (2010). Finite difference based calibration and simulation.

Black, F., & Scholes, M. (1973). The pricing of options and corporate liabilities. *Journal of Political Economy*, *81*, 637–654.

Clark, I. (2011). Foreign exchange option pricing: A practitioners guide. West Sussex: Wiley.

Cozzi, D. (2012). Local stochastic volatility models. Solving the smile problem with a nonlinear partial integro-differential equation.

Dupire, B. (1994). Pricing with a smile. *Risk Magazine*, *7*, 18–20.

Engelmann, B., Koster, F., & Oeltz, D. (2012). Calibration of the heston stochastic local volatility model: A finite volume scheme. Available online, Ecole Centrale Paris.

Fengler, M. (2005). Semi-parametric modeling of implied volatility. Lecture notes. Berlin: Springer.

Glasserman, P. (2003). *Monte Carlo methods in financial engineering*. New York: Springer.

Göttker, S. J., & Spanderen, K. (2014). Stochastic local volatility in quantlib.

Hagan, B., Dumar, D., Lesniewski, A., & Woodward, D. (2002). Managing smile risk. *Wilmott Magazine*, *7*, 84–108.

Heston, S. (1993). A closed-form solution for options with stochastic volatility with applications to bond and currency options. *Review of Financial Studies*, *6*, 327–343.

Hout, K. J., & Foulon, S. (2010). ADI finite difference schemes for option pricing in the heston model with correlation. *International Journal of Numerical Analysis and Modeling*, *7*, 303–320.

Lucic, Z. (2013). Alternate direction implicit method for a stochastic local volatility model: High performance computing platforms comparison.

Ren, Y., Dilip, M., & Qian, M. (2007). Calibrating and pricing with embedded local volatility models. *Risk Magazine*, *20*, 138.

Tachet, R. (2011). Non-parametric model calibration in finance. Ph.D. thesis, Ecole Centrale Paris.

Tataru, G., & Fisher, T. (2010). *Stochastic local volatility*. Bloomberg.

Tian, Y. (1993). Hybrid stochastic-local volatility model with applications in pricing FX options. Ph.D. thesis, Monash University.

Van, A., Gryelak, L., & Oosterlee, C. (2014). The heston stochastic-local volatility model: efficient monte carlo simulation. *International Journal of Theoretical and Applied Finance*.